

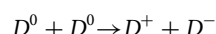
Spin blockade and exchange in Coulomb-confined silicon double quantum dots

Bent Weber¹, Y. H. Matthias Tan², Sudhasatta Mahapatra^{1†}, Thomas F. Watson¹, Hoon Ryu³, Rajib Rahman², Lloyd C. L. Hollenberg⁴, Gerhard Klimeck² and Michelle Y. Simmons^{1*}

Electron spins confined to phosphorus donors in silicon are promising candidates as qubits¹ because of their long coherence times, exceeding seconds in isotopically purified bulk silicon². With the recent demonstrations of initialization, readout³ and coherent manipulation⁴ of individual donor electron spins, the next challenge towards the realization of a Si:P donor-based quantum computer is the demonstration of exchange coupling^{1,5,6} in two tunnel-coupled phosphorus donors. Spin-to-charge conversion^{3,7} via Pauli spin blockade^{8,9}, an essential ingredient for reading out individual spin states, is challenging in donor-based systems due to the inherently large donor charging energies (~ 45 meV), requiring large electric fields (>1 MV m $^{-1}$) to transfer both electron spins onto the same donor¹⁰. Here, in a carefully characterized double donor-dot device, we directly observe spin blockade of the first few electrons and measure the effective exchange interaction between electron spins in coupled Coulomb-confined systems.

Scalable donor-based quantum-computing architectures envision arrays of donor spin qubits^{1,11} in which both single- and two-qubit operations are achieved by independently controlling each qubit using local magnetic¹² and electric¹³ fields. The path to scalability requires an understanding of the subtle and complex interplay between the electron's spin and charge degrees of freedom, for spin to charge conversion in qubit readout^{1,3,7,10}, for exchange coupling between qubits^{1,5,6} and for spin transport protocols^{14–16} requiring robustness against charge fluctuations. In this regard, donor-based spin qubits are distinguished by their strong Coulomb confinement, which, together with the symmetry properties of the silicon crystal, give rise to a low spin-orbit coupling^{6,10} and minimal interaction between spin and charge degrees of freedom.

Although spin-to-charge conversion via Pauli spin blockade has been achieved in few-electron double quantum dots in silicon and GaAs architectures^{7–9,17,18}, it is yet to be observed in tunnel-coupled pairs of donors^{19,20}, the fundamental building block of a scalable donor-based quantum-computing architecture. A key challenge in donor-based systems is the generation of a large enough electric field (>1 MV m $^{-1}$) between two tunnel-coupled donor dots separated by only ~ 10 nm to overcome the donor charging energies (~ 45 meV for single P donors). This allows the charge transfer of two electron spins onto the same donor dot, giving the following transition¹⁰:



Recent experiments in donor-defined double quantum dots have demonstrated electron transport¹⁹ and coherent manipulation of the charge degree of freedom²⁰, but to date, no signature of the spin degree of freedom has been reported. Here, we demonstrate the depletion of a Coulomb-confined few-donor double quantum dot down to the last electron, allowing the first demonstration of Pauli spin blockade in donor-based systems and allowing us to measure the effective exchange interaction.

The device consists of a planar scanning tunnelling microscope (STM)-patterned double-quantum-dot architecture (Fig. 1). Based on the STM images we can estimate an upper bound for the number of donors incorporated into each dot template. Consistent with the 0.25 monolayer (ML) doping density previously observed²¹, we can assume that one P atom incorporates into every two consecutive dimers and hence determine that up to two donors are incorporated into quantum dot D_1 and up to three into D_2 . Charge confinement in the device is provided solely by the presence of the ionized donors, causing a lowering of the local conduction band (CB) edge (E_{CB}). Within the quasi-metallic source/drain (S/D) leads, the local conduction band edge is located ~ 300 meV below the bulk silicon conduction band-edge with large Fermi energies of ~ 200 meV (ref. 22).

Figure 2a presents a charge stability diagram displaying the characteristic honeycomb stability diagram of a pair of tunnel-coupled quantum dots, in which each hexagonal domain corresponds to a stable electronic charge configuration (m,n) . Pairs of bias triangles, in which three adjacent charge states are degenerate, are highlighted by red and white circles. Here, electrons can tunnel freely from S to D through the sequence of charge states $(m,n) \rightarrow (m+1,n) \rightarrow (m,n+1) \rightarrow (m,n)$, provided such a sequence is permitted by spin selection rules. The total electron occupation (m,n) on each dot can be determined using finite bias spectroscopy measurements, shown in Fig. 2b. Here, we plot the logarithm of the differential conductance of the double dot as a function of S/D bias and V_{G2} , where $V_{G1} = 1.3V_{G2}$ (corresponding to the diagonal cut through the honeycomb stability map along the dashed red line in Fig. 2a), showing clear Coulomb blockade diamonds corresponding to tunnelling through both dots in series.

The electron numbers as well as the binding energies of the dots D_1 (D_2) are determined by the sequence and position of the parallel white (black) dashed lines bounding the CB diamonds at either S/D bias polarity in Fig. 2b. A crossing of either line slope at $V_D = 0$ reflects an alignment of the respective electrochemical potentials with the source (drain) Fermi levels²³ and a change in the electron

¹Centre of Excellence for Quantum Computation and Communication Technology, School of Physics, University of New South Wales, Sydney, New South Wales 2052, Australia. ²Network for Computational Nanotechnology, Birck Nanotechnology Center, Purdue University, 1205 West State Street, West Lafayette, Indiana 47907, USA. ³National Institute of Supercomputing and Networking, Korea Institute of Science and Technology Information, 245 Daehak-ro, Yuseong-gu, Daejeon 305-806, South Korea. ⁴Centre for Quantum Computation and Communication Technology, School of Physics, University of Melbourne, Parkville, Victoria 3010, Australia. [†]Present address: Department of Physics, Indian Institute of Technology Bombay, Powai, Mumbai 400076, India. *e-mail: michelle.simmons@unsw.edu.au

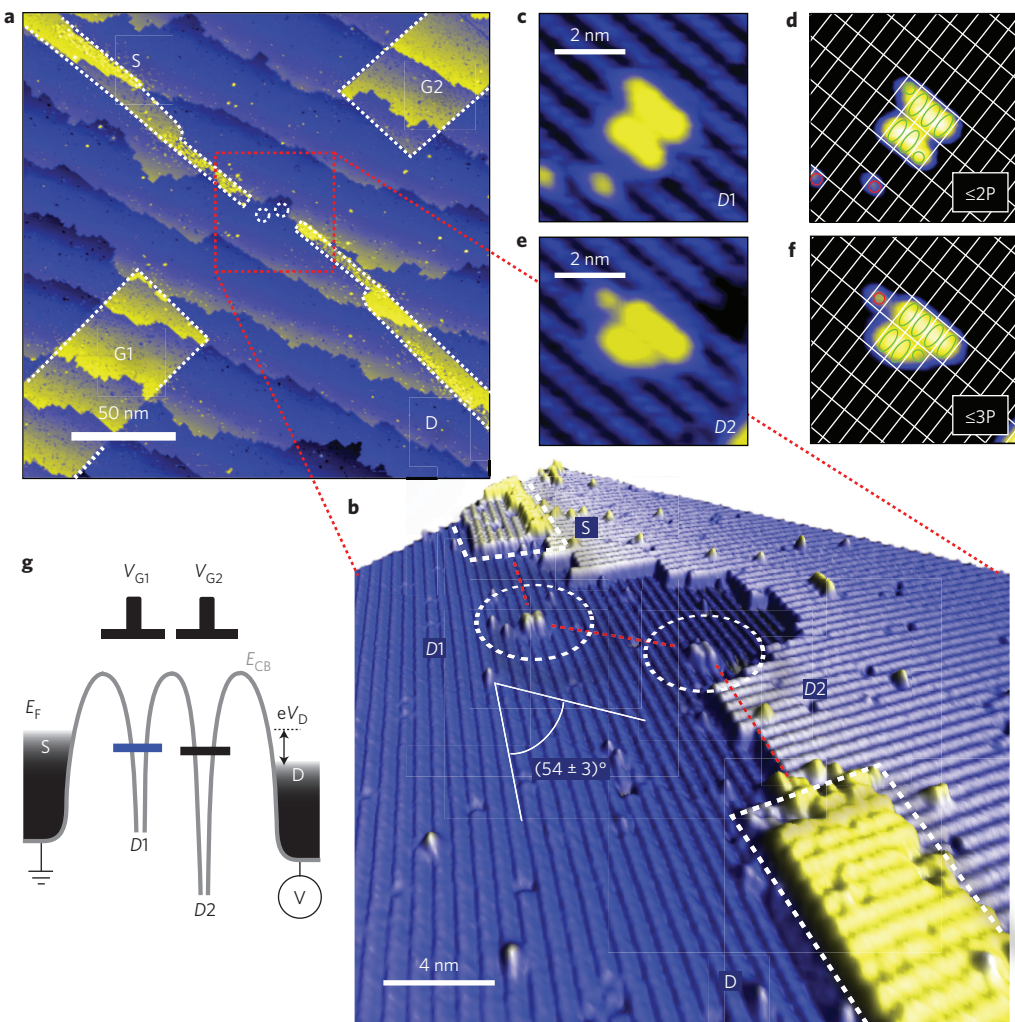


Figure 1 | A few-donor double quantum dot. **a**, STM images of a donor-based double-quantum-dot device template after STM lithography, showing source (S), drain (D) and gate (G1 and G2) electrodes. **b**, The central part of the device hosts two atomic-scale quantum dots (D1 and D2), symmetrically placed at a distance of 11.5 ± 0.5 nm between the S and D leads. The S and D electrodes are intentionally offset from each other, placing the dots at an angle of $\alpha = 54 \pm 3^\circ$ with respect to the source axis, to achieve independent gate control. **c–f**, Atomic-resolution STM images of D1 and D2 with the underlying Si(001)-2 \times 1 surface reconstruction. Both quantum dots extend across two adjacent dimer rows of the silicon surface with lengths of 2.5–4 contiguous dimers (green ellipses). Knowledge of the PH₃ dissociation and P incorporation pathway allows us to estimate the maximum number of incorporated donors in each dot: Up to two P in D1 and up to three P in D2 (assuming a 0.25 ML doping density²¹). No donors can incorporate into the single dangling bonds, highlighted by red circles. **g**, Schematic of the potential profile of the device defined by local variations of the silicon conduction band edge along a cut following the dashed red line in **b**. Charge confinement is given by a combination of individual donor Coulomb potentials tightly distributed within the dots.

occupation m and n on the respective dots. Consequently, we identify a total of two transitions on D1 and four transitions on D2. A simultaneous crossing of these lines at zero S/D bias ($V_{G2} \approx +400$ mV and $V_{G2} \approx +750$ mV) indicates two electrons being added, one to each dot, with the transitions offset in the gate voltage by the mutual Coulomb charging energy. At gate voltages of $V_{G2} < +400$ mV, no more charge transitions are observed on D1, consistent with its full depletion. Importantly, we also observe two further charge transitions on D2, reflected by the ‘kinks’ (points indicated by a diamond and a circle) at $V_{G2} \approx 200$ mV and $V_{G2} \approx 0$ mV. These characteristic features arise as electrons are removed from D2, resulting in a small downward shift of the D1 electrochemical potential due to the mutual Coulomb interaction²³. Notably, no more charge transitions on either D1 or D2 are observed down to gate voltages of $V_{G2} = -700$ mV and $|V_D| < 500$ mV, attesting to the full depletion of both dots.

Measuring the gate-voltage difference between the n th charge transitions (crossing of the white (black) dashed lines at $V_D = 0$) and the local conduction band edge E_{CB} (dotted red line in Fig. 2b) we can extract the binding energies, $E_{B,D1(2)}(n)$, of the n th bound electron, as summarized in Fig. 2c. The position of E_{CB} was determined at $V_{G2} = 870 \pm 10$ mV by plotting the logarithm of the current through the device versus the gate bias. From this, we take the intersection point of the onset of current and the background device current, that is, when the tunnel barriers are reduced to zero by the gates.

The binding energies extracted from two different directional cuts through the two-dimensional stability diagram ($V_{G1} = 1.3V_{G2}$ and $V_{G1} = V_{G2}$) are then compared with self-consistent atomistic tight-binding (TB) calculations, using NEMO-3D (Nanoelectronic Modelling tool)²⁴, for varying electron numbers on dots with different numbers of donors in Fig. 3. The binding energies are calculated

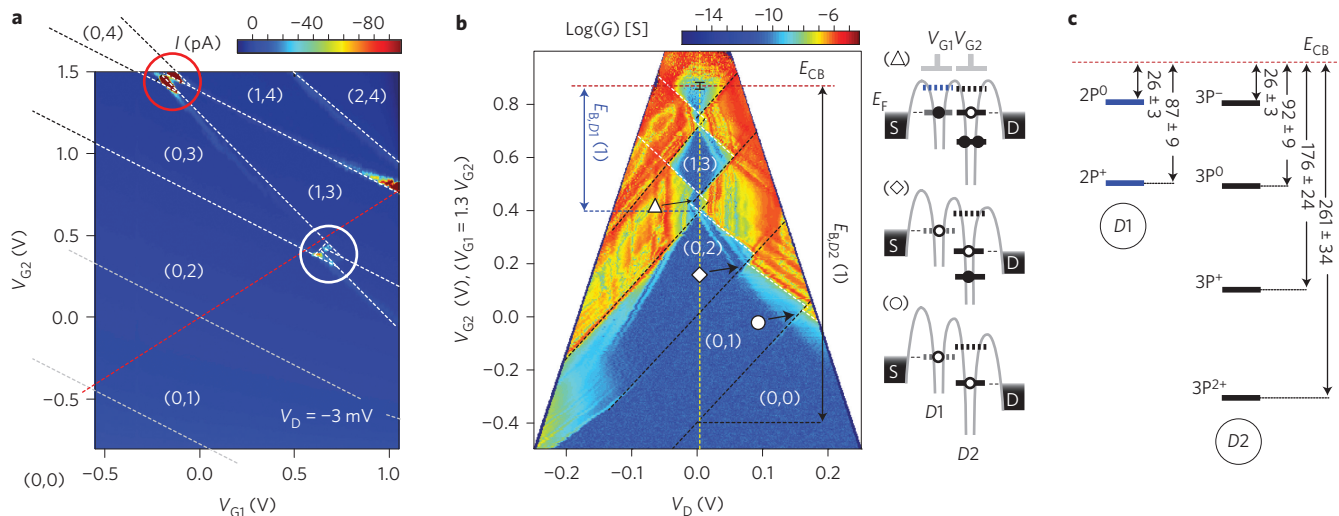


Figure 2 | Spectroscopy of a donor-based few-electron double quantum dot. **a**, Charge stability diagram ($V_D = -3$ mV) showing the drain current of the device as a function of both plunger gates G1 and G2, demonstrating independent electrostatic control over the individual dots. The red and white circles highlight finite bias triangles, investigated to demonstrate Pauli spin blockade in Fig. 4. **b**, The total electron numbers (n, m) as well as n -electron binding energies, $E_{B,D1(2)}(n)$, have been determined in finite bias spectroscopy measurements from a diagonal cut along the dashed red line in **a**. The accompanying schematics show the alignment of the respective dot electrochemical potentials as well as electron occupations at the three positions highlighted by a triangle, diamond and circle. The dashed white (black) lines bounding the Coulomb diamonds indicate the alignment of the D1 (D2) electrochemical potentials with the S (D) Fermi levels, respectively. The horizontal red dashed line in **b** indicates the approximate position of the silicon conduction band edge. **c**, Measured binding energy spectrum of D1 and D2.

by considering all possible donor configurations in each dot for every donor number, taking a lateral diffusion and vertical segregation of ~ 1 nm into account (see Supplementary Section 1). The resulting range of binding energies obtained for different donor configurations is indicated by the shaded bands, representing the percentile likelihood (%) of binding energies, based on inter-donor distance distribution functions (see Supplementary Section 1). For reference we also include NEMO calculations of the well-known binding energies of the D^0 (45.6 meV) and D^- (2 meV) states of an individual P donor²⁵ and compare these with those extracted experimentally from a previously published single donor device²⁶. As can be seen, these values independently confirm that we have a 2P donor dot in D1 and a 3P donor dot in D2, in agreement with the high-resolution STM images. These binding energies also compare well with those expected from a simple hydrogenic donor model (black horizontal arrows in Fig. 3),

$$E_n^Z = -13.6 \text{ eV} \left(\frac{Z^2 (m^*/m_e)}{\epsilon_{\text{Si}}^2} \right) \quad (1)$$

where Z is the donor number, $\epsilon_{\text{Si}} = 11.9$ is the dielectric constant of silicon and $m^* = 0.26m_e$ is the conductivity effective mass in silicon. From this we predict binding energies of 100 meV and 225 meV for the first electron bound to a 2P and 3P dot, respectively, which agree reasonably well with the measured single-electron binding energies of 87 ± 9 meV and 261 ± 34 meV. These results show that charge confinement is provided by the combined screened Coulomb potential of the closely spaced donor nuclei for a 2P and 3P donor dot, respectively.

Spin-to-charge conversion via Pauli spin blockade is well known in few-electron double quantum dots in silicon¹⁷ and GaAs^{8,9} architectures and arises from spin-selective tunnelling when each dot hosts a single unpaired spin. Tunnelling of both spins onto the same dot can only occur if the two spins are antiparallel (singlet) and is suppressed if they are parallel (triplet). This ultimately allows detection of the quantum state of the two-spin system. To investigate the spin degree of freedom in donor-confined quantum dots we return to the

two sets of bias triangles, highlighted by white and red circles in Fig. 2a. Close-ups of these transitions are shown in Fig. 4a,b, recorded at $V_D = \pm 5$ mV and ± 3 mV, respectively. As seen in the data, the first set of triangles at the $(1,2) \rightarrow (0,3)$ transition (white circle, Fig. 4a) is symmetric upon bias reversal, showing a well-pronounced ground-state resonance at the triangle base, as expected as a single, unpaired valence spin tunnels freely through both dots at either S/D bias polarity. In contrast, at the $(1,3) \rightarrow (0,4)$ transition (red circle, Fig. 4b) we find rectifying behaviour with a strong suppression of current at negative bias polarity. This provides a clear signature of spin blockade where at this transition only a single electron spin resides on D1 with an unpaired valence spin on D2 (Fig. 4b). Electron transport at this transition can therefore only proceed in the sequence $(0,3) \rightarrow (1,3) \rightarrow (0,4) \rightarrow (0,3)$ if both spins are antiparallel (that is, are in a singlet state). Current is blocked if the spins are aligned (that is, in a triplet state), with spin-selection rules prohibiting the occupancy of the $(0,4)$ charge state. As a result, the double quantum dot becomes stuck in a metastable spin triplet state, not allowing current from S to D. Clear lines of finite (~ 300 pA) current at the edges of the bias triangles in Fig. 4b arise when the $(1,3)$ spin states are within the thermal window of the source electrochemical potential, allowing spins to be exchanged with the S/D leads, lifting the blockade⁹.

This behaviour demonstrates Pauli spin blockade and even-odd filling as previously observed in few-electron GaAs/AlGaAs⁹ and silicon double quantum dots with lifted valley degeneracy^{17,18}. Although the spin filling sequence in silicon is theoretically predicted²⁷ to be complicated by orbital and valley degeneracies, even-odd filling has been observed²⁸ in tightly confined silicon dots ($d \approx 5$ nm) with large valley splitting and an anisotropic confinement potential. The atomistic TB calculations predict a valley-orbit gap on the order of meV depending on donor/electron number and precise donor distribution. For the atomic-scale few-donor dots presented here, the random physical distribution of donors within the size of a Bohr radius ($a_B \approx 2.5$ nm) leads to an absence of spatial symmetry, making even-odd spin filling likely.

Assuming a linear voltage drop between the $(1,2) \rightarrow (0,3)$ and $(1,3) \rightarrow (0,4)$ transitions we estimate a large transverse electric

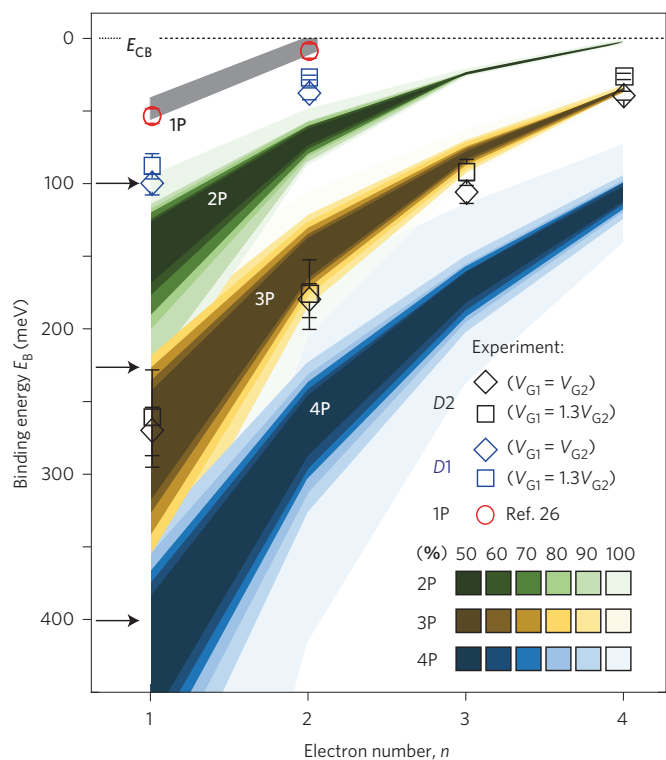


Figure 3 | Comparison of measured binding energy spectra of few-donor double quantum dots with self-consistent atomistic TB calculations. The measured spectra of D1 (blue diamond, $V_{G1} = V_{G2}$; blue square, $V_{G1} = 1.3V_{G2}$) and D2 (black diamond, $V_{G1} = V_{G2}$; black square, $V_{G1} = 1.3V_{G2}$), as well as a previously published single-atom transistor (red circle)²⁶ show good agreement with atomistic calculations of binding energy spectra. This allows identification of D1 and D2 as two- and three-P donor dots (shaded bands), showing clear differences with the known binding energy of a single-P donor. The widths of the shaded bands in the modelling reflect the respective variations in binding energies due to different spatial distributions of donors within each dot, taking a diffusion length of ~ 1 nm into account. Variations from these two directional cuts are less than the experimental error bars (± 3 meV to ± 34 meV), arising due to the uncertainty in the absolute position of E_{CB} and the lever arm, α . The lever arm for each cut was extracted from the diamond edges³⁰ at each charge transition and found to decrease slightly with increasing gate voltage from $\alpha = 0.22$ for the first electron on D2 to $\alpha = 0.18$ for the second (fourth) electron on D1 (D2). For each measured binding energy $E_{B,D1(2)}(n)$ we have therefore taken an average α over the range of gate voltages up to the respective transition.

field, $E \approx \Delta V_G/d \approx 9$ MV m⁻¹, applied by differential gate voltages between G1 and G2 (separated by $d = 150$ nm). This allows us to overcome the measured charging energy (63 ± 5 meV) given by the difference in binding energy between the (0,4) and (0,3) charge states, allowing both valence spins to tunnel onto D2 and giving rise to the observed spin blockade. At the (0,4) transition shown in Fig. 4c, we obtain an estimate for the effective singlet and triplet energy splitting $\Delta_{ST} = 8 \pm 1$ meV at large S/D bias ($V_D = \pm 13$ mV) with $\alpha_2 = 0.09$. This value is in reasonable agreement with theoretical estimates (~ 5.3 meV)¹⁰ for the singlet-triplet splitting of tunnel-coupled single donors, in the ionized (D^+/D^-) charge state. It is also up to two orders of magnitude larger than that typically observed for the first few electrons in silicon double quantum dots^{17,18}, due to the strong Coulomb confinement in donor-based systems¹⁰.

Finally, for donor-based quantum-computing architectures, it is important to gain an estimate of the strength of the effective exchange energy J between donor-bound spins. This can be

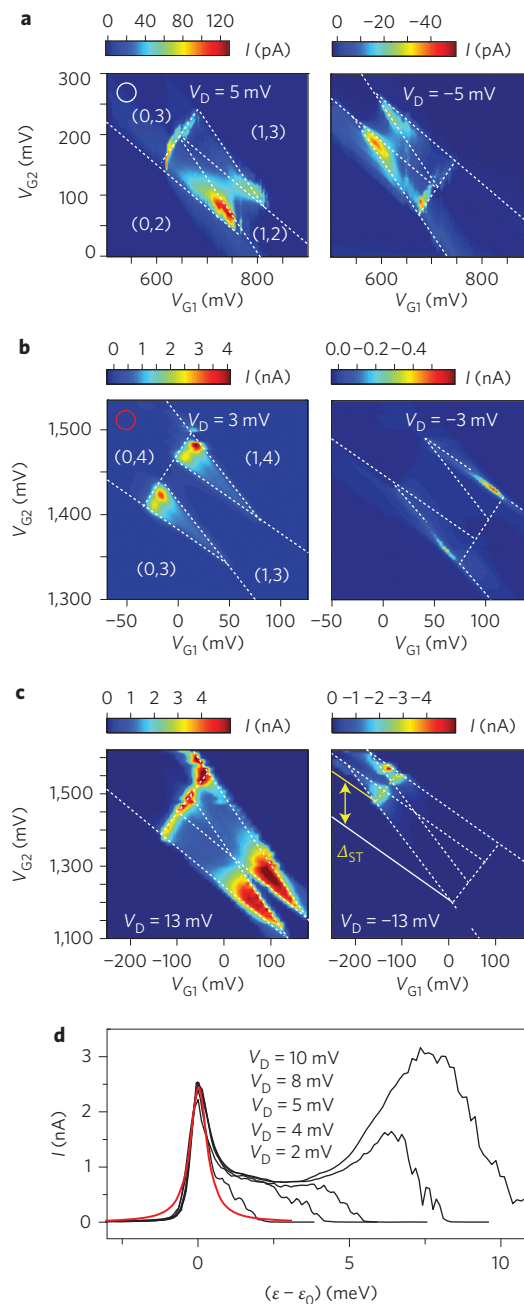


Figure 4 | Observation of spin blockade. **a,b**, Close-ups of the (1,2) \rightarrow (0,3) and (1,3) \rightarrow (0,4) transitions as highlighted by white and red circles, respectively, in Fig. 2a. Spin blockade is observed at the transition with an even electron number (**b**), involving a single spin on the D1 and an unpaired spin in D2. No blockade is observed at the odd electron numbers, supporting the conventional picture of spin blockade due to effective two-spin singlet and triplet states. Clear lines of current along the outer edges of the triangles result from spin exchange with the S/D electrodes. **c**, Measurement of the singlet-triplet splitting $\Delta_{ST} = 8 \pm 1$ meV. **d**, Fit to the ground-state resonance at positive bias to extract the mutual tunnel coupling. For resonant tunnelling through discrete states coupled in series, neither resonance current nor shape depend on applied bias or temperature, provided $eV_D \gg k_B T$ (ref. 19). A second resonance observed at large drain bias and positive detuning arises from resonant tunnelling once the (0,4) singlet state aligns with a higher-lying excited state in D1. Finite current between both resonances results from inelastic processes and co-tunnelling. (For this measurement the S and D terminals (see Methods) were reversed.)

obtained from the tunnel coupling strength at the $(1,3) \rightarrow (0,4)$ charge transition by fitting the ground-state resonance, shown in Fig. 4d for different values of S/D bias ($V_D > 0$). The expression^{19,29}

$$I(\varepsilon) = \frac{e\Gamma_D |t_c|^2}{\left(\frac{\hbar\Gamma_D}{2}\right)^2 + |t_c|^2 \left(2 + \frac{\Gamma_D}{\Gamma_S}\right) + (\varepsilon - \varepsilon_0)^2} \quad (2)$$

describes the resonance current across two discrete quantum states in two quantum dots D1 (D2) with energy difference $\varepsilon - \varepsilon_0$. From this we extract a mutual tunnel coupling, $t_c \approx 200 \mu\text{eV}$, between the dots as well as tunnel rates to the respective D (S) electrodes of $\Gamma_S \approx \Gamma_D \approx 50 \text{ GHz}$. At zero detuning, $\varepsilon = \varepsilon_0$, the effective exchange equals the tunnel coupling⁷. We therefore estimate an effective exchange interaction energy of $J \approx 200 \mu\text{eV}$, where the ground states of the (1,3) and (0,4) charge configurations align. We note that whilst a direct comparison to single donors is challenging due to the complexity of the multi-electron states in our system, we find this value to be comparable to theoretical estimates of the exchange energy for single donors in the (D^0/D^0) charge state⁵. This determination of the effective exchange energy therefore provides a first indication of the energy scale of electron spin coupling in donor-confined systems.

To summarize, we have observed Pauli spin blockade and exchange coupling in transport through a few-electron, donor double quantum dot. The two dots are composed of two (2P) and three (3P) donor atoms, placed with atomic-precision control within an all-epitaxial silicon device architecture. The precise donor and electron numbers were confirmed by finite bias spectroscopy, STM imaging and atomistic TB calculations. We have demonstrated that we can apply large enough electric fields to overcome the inherently large charging energies in donor dots to transfer both electron spins onto the same dot. Consequently, we observe spin blockade at the $(1,3) \rightarrow (0,4)$ charge transition, involving a single electron spin on the 2P dot that forms effective two-spin singlet and triplet states with an unpaired valence spin ($n = 3$) on the 3P dot. These results allow us to estimate the effective exchange interaction at the hybridization point between Coulomb-confined electron spins, providing an important step on the road to two-spin logic gates in donor-based quantum-computing architectures.

Methods

Device fabrication. The few-donor double quantum dot was realized using STM hydrogen lithography on the Si(001)-2 \times 1 reconstructed surface of an n-type ($\sim 1 \times 10^{15} \text{ cm}^{-3}$) silicon substrate, passivated with a monolayer of hydrogen resist¹³. The tip of an STM ($U = 4\text{--}7 \text{ V}$, $I = 3\text{--}5 \text{ nA}$) was used to locally desorb hydrogen atoms to define source (S), drain (D) and gate (G1 and G2) electrodes, as well as two small quantum dots (D1 and D2). Subsequent exposure to PH₃ gas with annealing (350°C) selectively doped the device template to $\sim 1/4 \text{ ML density}$ ($\sim 2 \times 10^{14} \text{ cm}^{-2}$), allowing quasi-metallic conduction in all electrodes^{22,26}. Following dopant incorporation, the device was overgrown with $\sim 25 \text{ nm}$ of epitaxial silicon at 250°C to minimize vertical segregation and lateral diffusion of the donors to $< 1 \text{ nm}$, before the *ex situ* alignment of aluminium ohmic contacts. In all subsequent electrical measurements, the electron occupation (n, m) on dots D1 (D2) was controlled by the respective plunger gates G1 (G2) while supplying a bias voltage to the D lead. Data were recorded over two separate cooldowns in a dilution refrigerator (electron temperature $T \approx 200 \text{ mK}$), during which the device remained reproducible.

Theoretical calculations. The Si:P donor-based quantum dots were modelled by constructing clusters of 2P, 3P and 4P donor atoms distributed at substitutional lattice sites within the lithographically defined quantum dot (Fig. 1c-f) and were embedded within a $30 \times 30 \times 30 \text{ nm}^3$ simulation domain of atomistic representation. Donor diffusion was also included into the modelling by taking into account diffusion of donors by $\sim 1 \text{ nm}$ in all directions (see Supplementary Sections 2 and 3). Each individual donor was represented by a screened and truncated Coulomb potential at a substitutional lattice site, which was parameterized to give the experimental ground-state energy of 45.6 meV for Si:P (ref. 25). The method applied to the calculation of the two-electron D⁻ energy provided $\sim 2 \text{ meV}$ binding energy, in close agreement with the experiments. The n -electron ground-state energies for different donor dots were subsequently obtained through self-

consistent charge-potential Schrödinger–Poisson calculations, with electron–electron interaction effects taken into account through a local density approximation (LDA) ansatz. Binding energies are expressed with respect to the silicon bulk conduction band edge E_{CB} .

Received 20 October 2013; accepted 26 February 2014;
published online 13 April 2014

References

- Kane, B. E. A silicon-based nuclear spin quantum computer. *Nature* **393**, 133–137 (1998).
- Tyryshkin, A. M. *et al.* Electron spin coherence exceeding seconds in high-purity silicon. *Nature Mater.* **11**, 143–147 (2012).
- Morello, A. *et al.* Single-shot readout of an electron spin in silicon. *Nature* **467**, 687–691 (2010).
- Pla, J. J. *et al.* A single-atom electron spin qubit in silicon. *Nature* **489**, 541–545 (2012).
- Koiller, B., Hu, X. & Das Sarma, S. Exchange in silicon-based quantum computer architecture. *Phys. Rev. Lett.* **88**, 027903 (2001).
- Wellard, C. J. *et al.* Electron exchange coupling for single-donor solid-state spin qubits. *Phys. Rev. B* **68**, 195209 (2003).
- Petta, J. R. *et al.* Coherent manipulation of coupled electron spins in semiconductor quantum dots. *Science* **309**, 2180–2184 (2005).
- Ono, K., Austing, D. G., Tokura, Y. & Tarucha, S. Current rectification by Pauli exclusion in a weakly coupled double quantum dot system. *Science* **297**, 1313–1317 (2002).
- Johnson, A. C., Petta, J. R., Marcus, C. M., Hanson, M. P. & Gossard, A. C. Singlet-triplet spin blockade and charge sensing in a few-electron double quantum dot. *Phys. Rev. B* **72**, 165308 (2005).
- Fang, A., Chang, Y. C. & Tucker, J. R. Effects of J-gate potential and uniform electric field on a coupled donor pair in Si for quantum computing. *Phys. Rev. B* **66**, 155331 (2002).
- Hollenberg, L. C. L., Greentree, A. D., Fowler, A. G. & Wellard, C. J. Two-dimensional architectures for donor-based quantum computing. *Phys. Rev. B* **74**, 045311 (2006).
- Büch, H., Mahapatra, S., Rahman, R., Morello, A. & Simmons, M. Y. Spin readout and addressability of phosphorus-donor clusters in silicon. *Nature Commun.* **4**, 2017 (2013).
- Weber, B., Mahapatra, S., Watson, T. F. & Simmons, M. Y. Engineering independent electrostatic control of atomic-scale ($\sim 4 \text{ nm}$) silicon double quantum dots. *Nano Lett.* **12**, 4001–4006 (2012).
- Greentree, A. D., Cole, J. H., Hamilton, A. R. & Hollenberg, L. C. L. Coherent electronic transfer in quantum dot systems using adiabatic passage. *Phys. Rev. B* **70**, 235317 (2004).
- Bose, S. Quantum communication through spin chain dynamics: an introductory overview. *Contemp. Phys.* **48**, 13 (2007).
- Skinner, A. J., Davenport, M. E. & Kane, B. E. Hydrogenic spin quantum computing in silicon: a digital approach. *Phys. Rev. Lett.* **90**, 087901 (2003).
- Shaji, N. *et al.* Spin blockade and lifetime-enhanced transport in a few-electron Si/SiGe double quantum dot. *Nature Phys.* **4**, 540–544 (2008).
- Borselli, M. G. *et al.* Measurement of valley splitting in high-symmetry Si/SiGe quantum dots. *Appl. Phys. Lett.* **98**, 123118 (2011).
- Roche, B. *et al.* Detection of a large valley-orbit splitting in silicon with two-donor spectroscopy. *Phys. Rev. Lett.* **108**, 206812 (2012).
- Dupont-Ferrier, E. *et al.* Coherent coupling of two dopants in a silicon nanowire probed by Landau-Zener-Stückelberg interferometry. *Phys. Rev. Lett.* **110**, 136802 (2013).
- Warschkow, O. *et al.* Phosphine adsorption and dissociation on the Si(001) surface: An ab initio survey of structures. *Phys. Rev. B* **72**, 125328 (2005).
- Weber, B. *et al.* Ohm's law survives to the atomic scale. *Science* **335**, 64–67 (2012).
- Führer, A. *et al.* Few electron double quantum dots in InAs/InP nanowire heterostructures. *Nano Lett.* **7**, 243–246 (2006).
- Klimeck, G. *et al.* Atomistic simulation of realistically sized nanodevices using NEMO 3-D – part I: models and benchmarks. *IEEE Trans. Electron. Dev.* **54**, 2079–2089 (2007).
- Rahman, R. *et al.* High precision quantum control of single donor spins in silicon. *Phys. Rev. Lett.* **99**, 036403 (2007).
- Fuechsle, M. *et al.* A single-atom transistor. *Nature Nanotech.* **7**, 242–246 (2012).
- Hada, Y. & Eto, M. Electronic states in silicon quantum dots: multivalley artificial atoms. *Phys. Rev. B* **68**, 155322 (2003).
- Lim, W. H., Yang, C. H., Zwanenburg, F. A. & Dzurak, A. S. Spin filling of valley-orbit states in a silicon quantum dot. *Nanotechnology* **22**, 335704 (2011).
- Nazarov, Y. V. Quantum interference, tunnel junctions and resonant tunneling interferometer. *Physica B* **189**, 57 (1993).
- Badrutdinov, A., Huang, S., Kono, K., Ono, K. & Tayurskii, D. Cotunneling effects in GaAs vertical double quantum dots. *JETP Lett.* **93**, 199–202 (2011).

Acknowledgements

This research was conducted by the Australian Research Council Centre of Excellence for Quantum Computation and Communication Technology (project no. CE110001027) and the US National Security Agency and US Army Research Office (contract no. W911NF-08-1-0527). Computational resources on nanoHUB.org, funded by the National Science Foundation (grant no. EEC-0228390), were used extensively. M.Y.S. acknowledges an ARC Laureate Fellowship.

Author contributions

B.W. and T.F.W. carried out the fabrication. B.W. performed measurements. B.W., Y.H.M.T., S.M., T.F.W., H.R., R.R., L.H., G.K. and M.Y.S. analysed the data. Y.H.M.T., H.R.

and R.R. carried out the calculations. M.Y.S. planned the project. G.K. planned the theoretical modelling approach. B.W. and M.Y.S. prepared the manuscript.

Additional information

Supplementary information is available in the [online version](#) of the paper. Reprints and permissions information is available online at [www.nature.com/reprints](#). Correspondence and requests for materials should be addressed to M.Y.S.

Competing financial interests

The authors declare no competing financial interests.